Biol. Chem., Vol. 388, pp. 705–715, July 2007 • Copyright © by Walter de Gruyter • Berlin • New York. DOI 10.1515/BC.2007.088

Long-range impact of peripheral joining elements on structure and function of the hepatitis delta virus ribozyme

Rebecca A. Tinsley and Nils G. Walter*

Department of Chemistry, University of Michigan, 930 N. University Ave., Ann Arbor, MI 48109-1055, USA

*Corresponding author
e-mail: nwalter@umich.edu

Abstract

The HDV ribozyme is an RNA enzyme from the human pathogenic hepatitis delta virus (HDV) that has recently also been identified in the human genome. It folds into a compact, nested double-pseudoknot. We examined here the functional relevance of the capping loop L4 and the helical crossover J1/2, which tightly interlace the two helical stacks of the ribozyme. Peripheral structural elements such as these are present in *cis*-acting, but not *trans*-acting ribozymes, which may explain the order-of-magnitude decrease in cleavage activity observed in *trans*-acting ribozymes with promise in gene therapy applications. Comparison of a systematic set of *cis*- and *trans*-acting HDV ribozymes shows that the absence of either L4 or J1/2 significantly and independently impacts catalytic activity. Using terbium(III) footprinting and affinity studies, as well as distance measurements based on time-resolved fluorescence resonance energy transfer, we find that J1/2 is most important for conferring structural properties similar to those of the *cis*-acting ribozyme. Our results are consistent with a model in which removal of either a helical crossover or surprisingly a capping loop induces greater dynamics and expansion of the catalytic core at long range, impacting local and global folding, as well as catalytic function.

Keywords: gene therapy applications; global folding; RNA catalysis; terbium(III) footprinting; time-resolved FRET.

Introduction

Our increased understanding of RNA enzymes (ribozymes) has led to their application as potential gene therapeutic agents for the intracellular suppression of viral pathogens and other disease-related genes (Sullenger and Gilboa, 2002; Breaker, 2004). In gene therapy, small endonucleolytic ribozymes may be used to bind target RNAs through specific base-pairing, cleaving them and releasing disabled products; this process can be repeated multiple times through catalytic turnover (Sullenger and Gilboa, 2002). To apply such a ribozyme successfully, the naturally occurring, self-(*cis*-)cleaving form must be modified into a *trans*-cleaving version to bind and cleave an external target strand with a cleavage rate that surpasses the ribozyme's intracellular degradation rate (Breaker, 2004). Indeed, several naturally occurring ribozymes, including the hammerhead and hairpin ribozymes, have shown sufficient promise during *in vitro* studies to be introduced in clinical trials (Sullenger and Gilboa, 2002). Other members of the class of small ribozymes, which are all under 200 nucleotides in length and share a common reaction chemistry, are the hepatitis delta virus (HDV) and *Neurospora* Varkud satellite ribozymes (Lilley, 2004; Winkler et al., 2004; Doudna and Lorsch, 2005; Fedor and Williamson, 2005), providing a structurally diverse pool of potential gene therapeutic agents.

HDV is a small pathogenic RNA satellite of the hepatitis B virus (HBV). Coinfection with HDV and HBV often leads to intensification of the disease symptoms associated with HBV, such as liver cirrhosis. The genome of HDV RNA is single-stranded and circular, with approximately 1700 nucleotides. It contains a high degree of intramolecular base pairing (approx. 70%), which results in the formation of an unbranched rod-like structure under physiological conditions. The HDV genome is approximately four- to five-fold longer than a typical viroid RNA and encodes a unique protein, the delta antigen. Double-rolling circle replication of HDV is dependent on self-cleavage of the genomic and complementary antigenomic RNAs, which is mediated in both strands by a nearly identical HDV ribozyme motif (Lai, 1995; Shih and Been, 2002; Been, 2006; Macnaughton and Lai, 2006). The recent discovery of a similar RNA motif in the human *CPEB3* gene raises the intriguing possibility that HDV may have arisen from the human transcriptome (Salehi-Ashtiani et al., 2006).

The fact that the HDV ribozyme is the only known endonucleolytic RNA to naturally function in human cells makes it a particularly promising gene therapeutic agent. In prior work, we devised a well-behaving *trans*-acting HDV ribozyme and characterized its structure-function relationships (Harris et al., 2002; Pereira et al., 2002; Jeong et al., 2003; Tinsley et al., 2003, 2004; Gondert et al., 2006; Sefcikova et al., 2007a). In particular, we performed fluorescence resonance energy transfer (FRET) assays on this HDV ribozyme and showed that a significant global conformational change accompanies catalysis (Harris et al., 2002; Pereira et al., 2002; Jeong et al., 2003; Tinsley et al., 2004). A similar, if somewhat muted, global extension along the P2–P4 axis was subsequently found to distinguish crystal structures of precursor and 3′-products forms of the *cis*-acting genomic HDV ribozyme, where this conformational switch is proposed to control catalysis (Ke et al., 2004; Tinsley et al., 2004). Our solution footprinting studies of the *cis*-acting antigenomic HDV ribozyme, which, like the genomic form, has a fast cleavage rate constant of ca. 30 min^{-1} (Perrotta and Been, 1998; Perrotta et al., 1999), demonstrated that it undergoes a similar conformational switch to that proposed for the genomic ribozyme (Harris et al., 2004).

Despite their similar structural behavior, *trans*-acting ribozyme variants generally show approximately 10- to 100-fold lower cleavage activity than their naturally occurring *cis*-acting genomic and antigenomic counterparts, a phenomenon that is ill understood (Pereira et al., 2002; Shih and Been, 2002; Tinsley et al., 2004). Given the importance of efficient *trans*-acting HDV ribozymes for potential gene therapeutic applications (Roy et al., 1999; D'Anjou et al., 2004; Fiola et al., 2006; Lucier et al., 2006), we set out to determine the reason for this activity loss. The major difference between *trans*- and *cis*-acting ribozymes is the lack of the native closing loop L4 and/or helical crossover J1/2 in the former, structural elements that help to interlace the top and bottom of the parallel P2–P3 and P1–P1.1–P4 helical stacks, respectively (Figure 1). We hypothesized that the absence of these joining strands may result in relaxation and larger fluctuations of the P2–P4 end-to-end distance and/or angle of the P2–P3 stack relative to P1–P1.1–P4. Such global structural rearrangements may then lead to a less tightly folded catalytic core and slower cleavage.

To test our hypothesis, we generated a systematic set of *trans*-acting constructs based on the antigenomic *cis*-acting HDV ribozyme construct PEX-1 used in several previous studies (Perrotta and Been, 1998; Perrotta et al., 1999; Shih and Been, 2001; Wadkins et al., 2001; Harris et al., 2004). The new ribozyme constructs are identical in sequence to PEX-1, except that they lack the strand connections represented by loop L4 and/or joiner J1/2, so that they become two- or three-strand *trans*-acting HDV ribozymes. We observed significant differences in cleavage activity between the four constructs. Loss of L4 and J1/2 led to an ~15- and ~24-fold decrease in catalytic activity, respectively. Loss of both elements together led to an approximately 127-fold decrease in activity, suggesting that both structural elements function in a

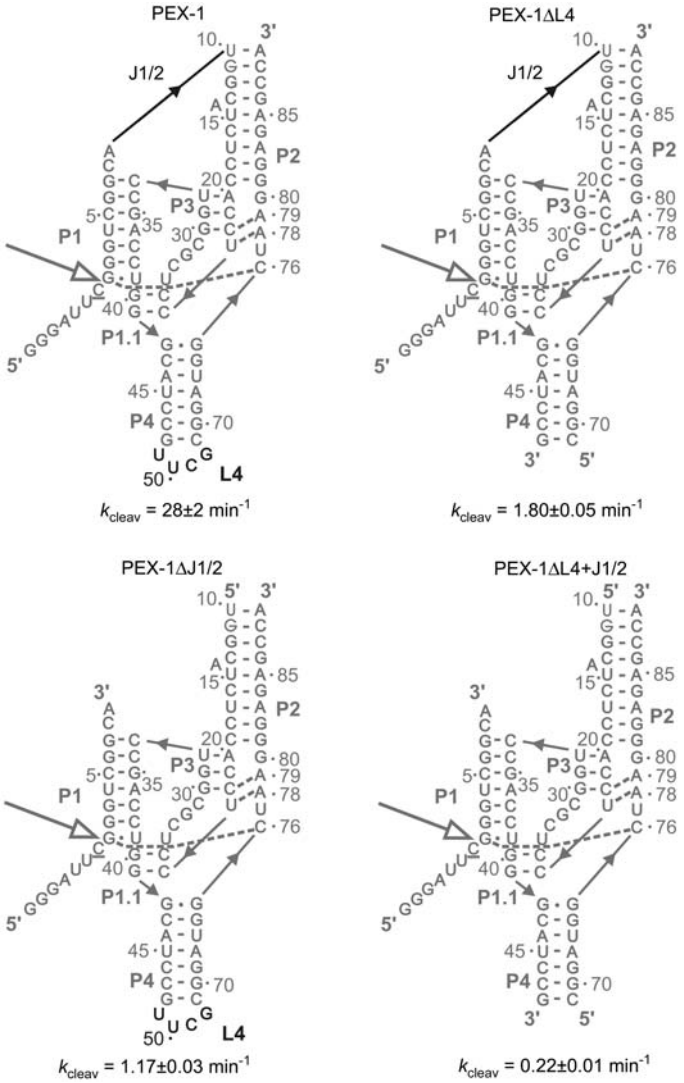

Figure 1 Secondary structure of the *cis*- and *trans*-acting antigenomic HDV ribozymes used in this study.
All *trans*-acting constructs originate from the parent *cis*-acting construct PEX-1. In the PEX-1ΔL4 construct, loop L4 has been removed, while in the PEX-1ΔJ1/2 construct, the helical crossover J1/2 has been removed to form two-strand constructs. Construct PEX-1ΔL4+J1/2 contains neither J1/2 nor L4. To maintain the previously defined antigenomic numbering system, we numbered the nucleotides downstream of the L4 loop as shown. Non-cleavable precursor forms were generated by modifying the 2′-OH group of the underlined nucleotide 5′ to the cleavage site (open arrow) to 2′-methoxy during chemical synthesis. Listed below each construct is the single-turnover cleavage rate constant under standard conditions (25 mM acetic acid, 25 mM MES, 50 mM Tris-HCl, pH 7.5, 11 mM $MgCl_2$, at 37°C) with standard deviation for at least three independent determinations.

largely independent fashion. Using Mg^{2+}-dependent cleavage, terbium(III)-mediated footprinting and luminescence, we show that the construct that contains the helical crossover J1/2 but lacks L4 has Mg^{2+} and Tb^{3+} binding affinities more similar to those of the *cis*-acting PEX-1 than does a construct lacking J1/2. In addition, time-resolved FRET revealed that joiner J1/2 is responsible for muting the global conformational switch from precursor to product. Our data support the notion that the joining elements act to connect the helical stacks tightly; without them, the HDV ribozyme has a more open tertiary structure that requires higher Mg^{2+} concentrations for folding and is less conducive to catalytic activity. This may be most surprising for the distal capping loop L4.

Results

Removal of either loop L4 or joiner J1/2 decreases cleavage activity in a largely independent fashion

Figure 1 shows the systematic set of *cis*- and *trans*-acting HDV ribozymes of the present study, which are based on the antigenomic HDV ribozyme construct PEX-1 used previously (Perrotta and Been, 1998; Perrotta et al., 1999; Shih and Been, 2001; Wadkins et al., 2001; Harris et al., 2004); it should be noted that we omitted the vector-derived 5-nucleotide sequence 5′-GGUAC-3′ found on the 3′-end of the original PEX-1. Three *trans*-acting constructs were generated that are almost identical to PEX-1: PEX-1ΔL4 contains the helical crossover J1/2 that connects the tops of helices P1 and P2, but lacks loop L4; PEX-1ΔJ1/2 contains loop L4, which caps the bottom of P4, but J1/2 was severed; and PEX-1ΔL4+J1/2 is a three-strand construct containing neither L4 nor J1/2. To compare the single-turnover cleavage activity of these constructs under equivalent conditions, a protocol optimized for the PEX-1 construct was adapted for all four constructs (Wadkins et al., 2001; Harris et al., 2004). Briefly, radiolabeled reaction precursor PEX-1 (5–50 nM) or trace (<1 nM) amounts of radiolabeled substrate with varying excess concentrations of *trans*-acting ribozyme were heated to 90°C for 3 min in a buffer of 5 mM Tris-HCl, pH 7.5, 0.5 mM spermidine. After incubation at 37°C for 10 min, standard buffer [25 mM acetic acid, 25 mM 2-(*N*-morpholino)ethane sulfonic acid (MES), 50 mM Tris-HCl, pH 7.5] was added. Reactions at 37°C were initiated by the addition of Mg^{2+} to a final concentration of 11 mM and aliquots were analyzed by denaturing gel electrophoresis. For PEX-1, the fraction cleaved was plotted as a function of time and fit to yield a first-order rate constant, k_{cleav}, of 28±2 min^{-1} (fraction cleaved approx. 70%). For the three *trans*-acting constructs, the observed rate constants, k_{obs}, were plotted as a function of ribozyme concentration and fit to yield a rate constant for the limiting step of cleavage at saturating ribozyme concentration, k_{cleav}, of 1.80±0.05 (fraction cleaved ca. 70%), 1.17±0.03 (70%), and 0.22±0.01 min^{-1} (50%) for PEX-1ΔL4, PEX-1ΔJ1/2, and PEX-1ΔL4+J1/2, respectively. Thus, the constructs are ~15-, ~24- and ~127-fold, respectively, less catalytically active than the parent *cis*-acting ribozyme (Figure 1). Notably, the loss in activity for the doubly modified construct PEX-1ΔL4+J1/2, lacking both P4 and J1/2, is equivalent to an apparent transition-state free energy increase of $\Delta\Delta G^{\ddagger}$=3.2 kcal/mol relative to the parent ribozyme, which is greater than the losses for both of the singly modified constructs PEX-1ΔL4 ($\Delta\Delta G^{\ddagger}$=1.8 kcal/mol) and PEX-1ΔJ1/2 ($\Delta\Delta G^{\ddagger}$=2.1 kcal/mol). This observation suggests that the effects of the two modifications are largely additive and thus independent. (Note that the differences in rates could be due to a change in the rate-limiting step between constructs, see the discussion.)

Gel mobility shift assay demonstrates homogeneity for all ribozyme constructs and suggests slightly less compact folding of constructs lacking joiner J1/2

To ensure homogeneity and detect structural distinctions in our ribozyme constructs, we performed a radioactive gel mobility shift assay. We found that all fully assembled ribozymes in both their non-cleavable (nc) precursor and 3′-product (3′P) forms (lacking the sequence 5′ of the cleavage site, i.e., the 5′-substrate; Figure 1) migrate as homogeneous single bands (Figure 2). In all cases, the precursor form migrates more slowly than the corresponding 3′P form, consistent with the notion that the 5′-substrate decreases the hydrodynamic mobility of the RNA. In the case of PEX-1 and PEX-1ΔL4, this mobility difference is very subtle, suggesting that their precursor and 3′P forms have quite similar folds. These two constructs also migrate slightly faster than their PEX-1ΔJ1/2 and PEX-1ΔL4+J1/2 counterparts, consistent with an overall tighter, more compact fold. The free ribozymes of the latter two constructs (both ΔJ1/2B, representing the 3′-segment of PEX-1ΔJ1/2, and PEX-1A+PEX-1B, representing the assembled 5′- and 3′-segments of PEX-

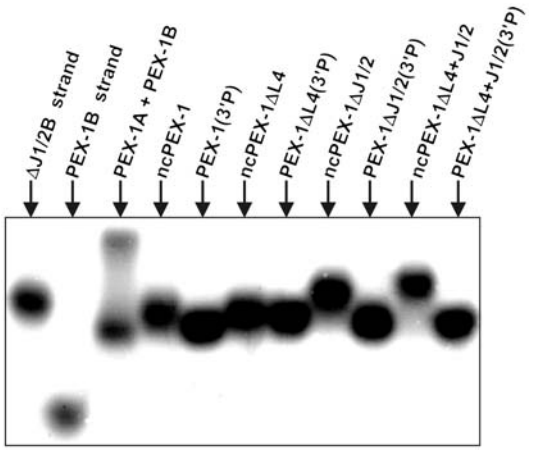

Figure 2 Non-denaturing gel mobility shift assay of our radiolabeled antigenomic HDV ribozyme constructs in both the non-cleavable (nc) precursor and 3′-product (3′P) forms.
Strand ΔJ1/2B represents the 3′-segment of the two-strand PEX-1ΔJ1/2 construct, while strand PEX-1A and PEX-1B represent the central and 3′-segments, respectively, of the PEX-1ΔL4+J1/2 construct (see Figure 1). The complex of PEX-1B+PEX-1A migrates in two bands, whereas all other complexes show a single homogeneous band. The precursor form generally migrates slightly more slowly than the respective 3′P form, as expected for a higher-molecular-mass complex.

1ΔL4+J1/2, respectively (Figure 2), nearly co-migrate with their assembled 3′P forms. In summary, our observations support the existence of homogeneously folding, structurally distinct precursor and 3′P structures for all four HDV ribozyme constructs, with the joiner J1/2-containing variants PEX-1 and PEX-1ΔL4 representing the most compact folds.

Catalytic metal ion affinity is lower for constructs lacking joiner J1/2

We measured the Mg^{2+} dependence of cleavage activity of our four HDV ribozyme constructs under standard single-turnover conditions. In the case of PEX-1, the observed rate constants increased from 0.2 to 28 min^{-1} between 50 μM and 11 mM $MgCl_2$, yielding a Mg^{2+} half-titration point, $Mg_{1/2}$, of 0.8±0.1 mM (cooperativity coefficient n=1.67, Table 1, Figure 3). The rate constant for PEX-1ΔL4 increased from 0.17 to 2.2 min^{-1} between 100 μM and 50 mM $MgCl_2$, yielding $Mg_{1/2}$ of 1.0±0.1 mM (n=1); that for PEX-1ΔJ1/2 increased from 0.1 to 1.93 min^{-1} between 500 μM and 200 mM, with $Mg_{1/2}$ of 9±1 mM (n=1.5); and that for PEX-1ΔL4+J1/2 increased from 0.01 to 0.87 min^{-1} between 1 and 400 mM $MgCl_2$, yielding $Mg_{1/2}$ of 60±6 mM (n=1). The apparent Mg^{2+} binding constants indicate that the magnesium affinity of PEX-1ΔL4 is within experimental error of that of the *cis*-acting PEX-1, while the PEX-1ΔJ1/2 and PEX-1ΔL4+J1/2 constructs bind magnesium with ca. 10- and 70-fold lower affinity, respectively. These observations suggest that joiner J1/2, present only in the PEX-1 and PEX-1ΔL4 constructs, plays an important role in the binding of catalytically essential Mg^{2+} ions.

Lack of joiner J1/2 renders the catalytic core of the precursor more susceptible to terbium(III)-induced backbone scission

High millimolar concentrations of terbium(III) can be used to slowly cut the RNA phosphodiester backbone in a largely sequence-independent manner, preferentially targeting single-stranded or non-Watson-Crick base-paired regions (Hargittai and Musier-Forsyth, 2000; Walter et al., 2000; Hargittai et al., 2001; Harris and Walter, 2003; Jeong et al., 2003; Harris et al., 2004). This property produces a footprint of RNA secondary and tertiary structure at nucleotide resolution, as exemplified in our previous work on the *cis*-acting PEX-1 antigenomic HDV ribozyme, for which we found subtle differences in the precursor and 3′P footprints consistent with the conformational switch observed in crystal structures of the genomic form (Harris et al., 2004). We therefore used terbium(III) to probe and compare the structures of our three *trans*-acting ribozymes, focusing on the catalytic core around nucleotide C76, which has been implicated as either the general base or acid during catalysis (Perrotta et al., 1999, 2006; Nakano et al., 2000; Das and Piccirilli, 2005).

To this end, trace amounts of the radiolabeled 3′-segment strand of PEX-1ΔL4, PEX-1ΔJ1/2, and PEX-1ΔL4+J1/2 were assembled with either nc substrate or 3′P under standard conditions in the presence of 11 mM Mg^{2+}, followed by addition of $TbCl_3$ to a final concentration of 1 mM to initiate slow backbone scission at 37°C

Table 1 Apparent magnesium ($Mg_{1/2}$) and terbium(III) half-titration points ($Tb_{1/2}$) for our four antigenomic HDV ribozyme constructs.

Construct	$Mg_{1/2}$ (mM)	$Tb_{1/2}(1)$ (μM)	$Tb_{1/2}(2)$ (μM)
PEX-1	0.8±0.1	5±2	21±2
PEX-1ΔL4	1.0±0.1	9±1	46±2
PEX-1ΔJ1/2	9±1	14±4	51±3
PEX-1ΔL4+J1/2	60±6	22±2	152±9

$Mg_{1/2}$ and $Tb_{1/2}$ values were measured under standard conditions as described in the materials and methods section. The corresponding data fits are shown in Figure 3 for magnesium and Figure 5B for terbium(III). Errors report the fit accuracy.

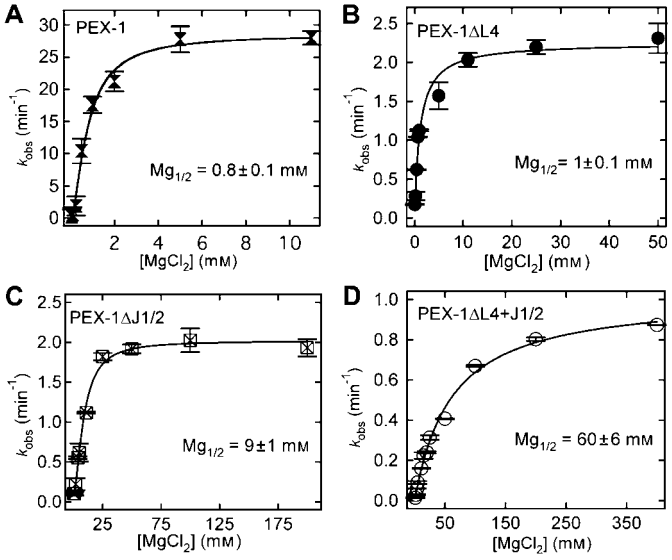

Figure 3 Observed cleavage rate constants, k_{obs}, as a function of Mg^{2+} concentration under standard conditions (25 mM acetic acid, 25 mM MES, 50 mM Tris-HCl, pH 7.5, at 37°C) for our four antigenomic HDV ribozyme constructs.
The experimental data were fit with binding Eq. (2) to yield the reported Mg^{2+} half-titration points $Mg_{1/2}$ (see also Table 1).

over 1 h. To compare footprinting patterns, the gel was quantified by linear cross-section, revealing the scission intensity for each nucleotide. These raw data were normalized to the scission intensity at G75 and plotted as a function of lane position, where each peak represents a nucleotide as indicated in Figure 4. As expected, the terbium(III)-protected and susceptible regions are similar between the precursor and 3′P for all constructs, consistent with an overall similar fold before and after catalysis. The scission patterns are also consistent with the expected secondary structure; the P2 and P4 helices are protected from terbium(III) scission relative to J4/2, a single-stranded joining segment. Strikingly, loop L4 of the precursor of the PEX-1ΔJ1/2 construct is significantly more strongly hit than L4 of the 3′P. Significant differences are also evident when the three constructs are compared. The terbium(III) scission patterns for J4/2 in the catalytic core of the PEX-1ΔL4 precursor and 3′P are more similar to one another than are the precursor and 3′P patterns of PEX-1ΔJ1/2 and PEX-1ΔL4+J1/2, which both lack joiner J1/2. This observation suggests that removal of J1/2 renders the catalytic core more sensitive to the presence of the 5′-sequence, enhancing terbium(III)-mediated scission of the A-minor motif interaction of A78 and A79 with helix P3 in the precursor structure (Figures 1 and 4).

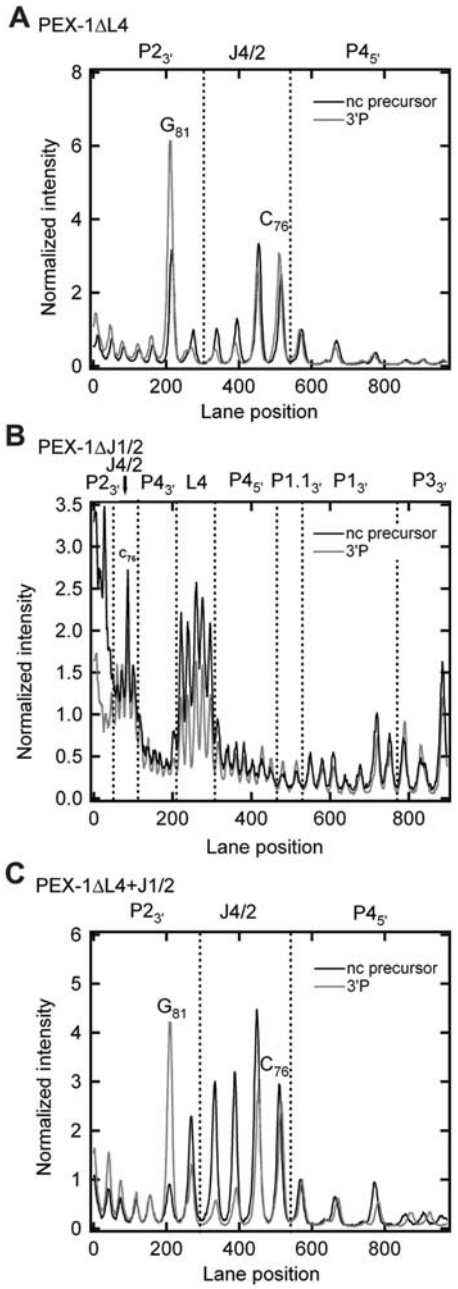

Figure 4 Intensity of terbium(III)-mediated backbone scission of our three *trans*-acting antigenomic HDV ribozyme constructs. Precursor (black) and 3′-product (grey) scission patterns of the radiolabeled 3′-segments of (A) PEX-1ΔL4, (B) PEX-1ΔJ1/2 and (C) PEX-1ΔL4+J1/2 after incubation for 1 h under standard conditions (25 mM acetic acid, 25 mM MES, 50 mM Tris-HCl, pH 7.5, 11 mM $MgCl_2$, at 37°C) in the presence of 1 mM Tb^{3+}, normalized to nucleotide G75.

Removal of either joiner J1/2 or loop L4 decreases terbium(III) binding affinity in a largely independent fashion

Terbium(III), a lanthanide cation, emits sensitized luminescence when it binds proximal to chromophores such as RNA nucleobases that transfer excited-state energy to the ion. This distinctive spectroscopic property of terbium(III) can be used to probe metal ion affinity over an entire RNA structure (Walter et al., 2000; Harris and Walter, 2003; Jeong et al., 2003; Harris et al., 2004). Here, we examined and compared the binding affinities of terbium(III) to the 3′P forms of our four antigenomic HDV ribozyme constructs.

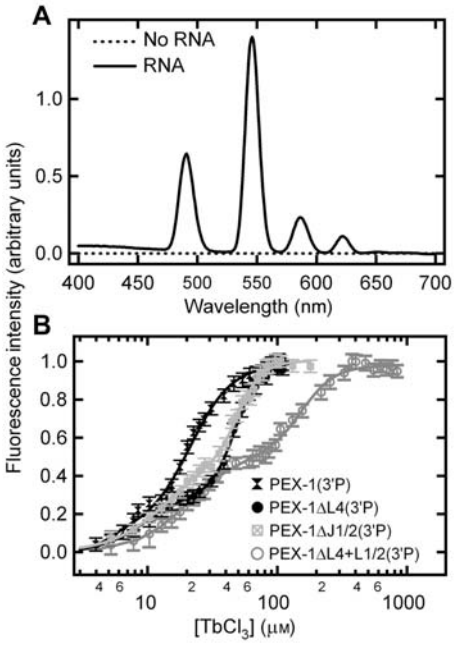

Figure 5 Sensitized terbium(III) luminescence spectroscopy of 1 μM 3′-product form of our four antigenomic HDV ribozyme constructs.
(A) Luminescence spectrum of 100 μM Tb^{3+} in the presence (solid line) and absence (dashed line) of the 3′-product of PEX-1, pre-folded in 11 mM $MgCl_2$ (see the materials and methods section). (B) Terbium(III) titration of each of the 3′-product forms in the presence of 11 mM Mg^{2+}, detected by the luminescence peak at 545 nm. The sum of two independent Hill functions [Eq. (3)] was fit to each data set, yielding two Tb^{3+} half-titration points $Tb_{1/2}$ (see also Table 1).

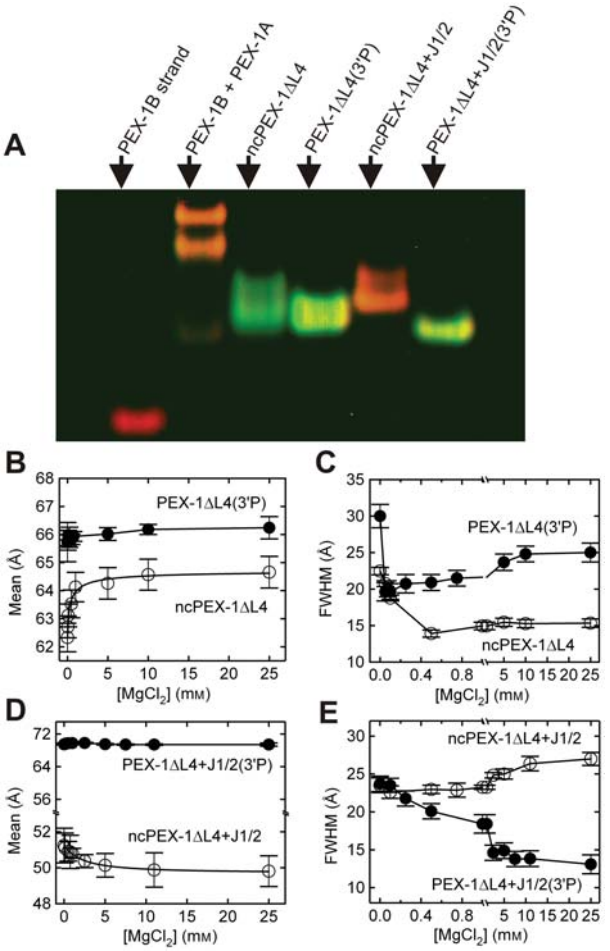

Figure 6 FRET analysis of the PEX-1ΔL4 and PEX-1ΔL4+J1/2 antigenomic HDV ribozyme constructs, differing in the integrity of joiner J1/2.

(A) Non-denaturing gel mobility shift assay of fluorescein-tetramethylrhodamine doubly labeled constructs, showing either green (donor)- or red (acceptor)-dominated FRET colors. The non-cleavable (nc) precursor forms run slightly more slowly than their respective 3′-product (3′P) forms (see also Figure 2). The substrate-free PEX-1ΔL4+J1/2 construct (PEX-1B+PEX-1A) migrates with multiple bands, where one band migrates close to the 3′P form, but can be distinguished by its FRET color. (B–E) Mg^{2+} dependence of the mean helix P2-P4 end-to-end distance and the associated full width at half-maximum (FWHM), as measured by time-resolved FRET, of antigenomic HDV ribozyme constructs PEX-1ΔL4 (panels B and D, respectively) and PEX-1ΔL4+J1/2 (panels C and E, respectively) in either the non-cleavable (nc) precursor or 3′P form.

Measurements were made in standard buffer (25 mM acetic acid, 25 mM MES, 50 mM Tris-HCl, pH 7.5) supplemented with 25 mM DTT at 37°C. The mean distances of nc PEX-1ΔL4 and ncPEX-1ΔL4+J1/2 were fit with binding Eq. (2) to yield Mg^{2+} half-titration points of 0.35±0.09 and 2.2±0.3 mM, respectively.

Addition of 100 μM Tb^{3+} to 1 μM 3′P form of the pre-annealed PEX-1ΔL4 construct in 11 mM $MgCl_2$ with excitation at 290 nm resulted in the emission spectrum shown in Figure 5A (continuous line). As expected (Walter et al., 2000; Harris and Walter, 2003; Jeong et al., 2003; Harris et al., 2004), four emission peaks are observed, with the most intense centered around 545 nm. In the absence of RNA, no such emission is observed (Figure 5A, dashed line). For each of our four HDV ribozymes, we measured the emission increase at 545 nm upon titration with terbium(III). The resulting curves are best fit to the sum of two independent Hill equations (see materials and methods), providing two terbium(III) half-titration points ($Tb_{1/2}$) for each construct (Table 1). The relative affinities of these generally observed two classes of terbium(III) ions thus follow the order PEX-1>PEX-1ΔL4>PEX-1ΔJ1/2>PEX-1ΔL4+J1/2, further supporting the notion that severing either loop L4 or joiner J1/2 independently weakens metal ion binding.

Lack of joiner J1/2 leads to higher Mg^{2+} requirement for global folding and amplification of the global conformational change accompanying catalysis

To further examine the role of joiner J1/2 in the global structure, we doubly-labeled the common PEX-1B strand of constructs PEX-1ΔL4 and PEX-1ΔL4+J1/2 with a 5′ fluorescein and 3′ tetramethylrhodamine.

To test the homogeneity of our doubly fluorophore-labeled constructs, we performed gel mobility shift assays. We found that the nc precursors of PEX-1ΔL4 and PEX-1ΔL4+J1/2 run with a slight lower-mobility smear, which may be due to a gel mobility that is averaged over a range of conformations. In the case of the PEX-1ΔL4 precursor, this observation appears consistent with the bimodal distance distribution detected by time-resolved FRET (see below). By comparison, both 3′P forms run as single homogeneous bands (Figure 6A). The relatively lower mobility of the precursors compared to their respective 3′P is consistent with the radioactive gel mobility shift assay in Figure 2. In our FRET gel, the precursor bands are red-shifted relative to their corresponding 3′P band, indicating higher FRET efficiency, although the difference is only very subtle in case of the joiner J1/2-containing PEX-1ΔL4 construct (Figure 6A). These findings are consistent with the more quantitative P2–P4 distance measurements from time-resolved FRET.

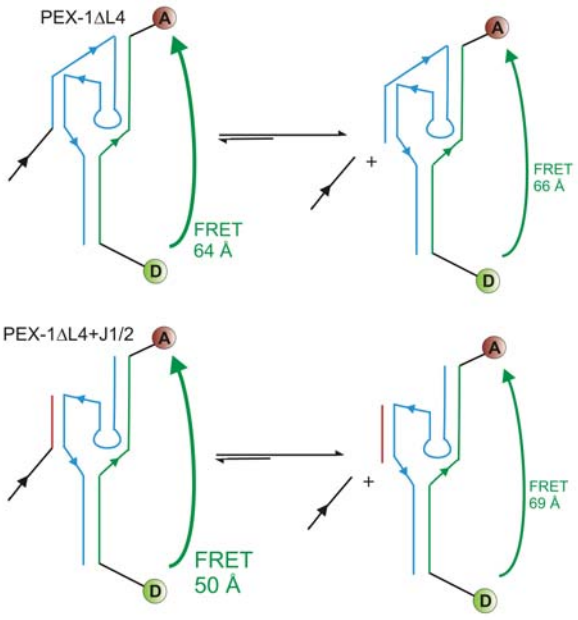

Figure 7 Summary of the global conformational changes upon *trans*-cleavage by the PEX-1ΔL4+J1/2 and PEX-1ΔL4 constructs.

Time-resolved FRET is a spectroscopic molecular ruler in which excitation energy is transferred in a distance-dependent manner from a donor to an acceptor fluorophore, judiciously placed on a biopolymer of interest. The distance between the fluorophores can be quantified to near-angstrom resolution to, for example, report on global structure, intrinsic flexibility, and/or alternate conformations of an RNA (Walter et al., 1999; Walter, 2001; Rueda et al., 2003). Figure 6B–D illustrates the Mg^{2+}-induced global conformational changes observed for the nc precursor and 3′P forms of constructs PEX-1ΔL4 and PEX-1ΔL4+J1/2 that share the same doubly labeled 3′-segment. The donor and acceptor are coupled to the 5′- and 3′-ends of the 3′-segment, respectively, to monitor the mean helix P2–P4 end-to-end distance in standard buffer at 37°C as a function of Mg^{2+} concentration. In all cases we obtained a single distance distribution from our time-resolved FRET analysis, except for the precursor of PEX-1ΔL4, for which we consistently observed a majority (80%) of the population centered around a mean distance of ca. 63 Å, with a small fraction (20%) centered around a mean distance of ca. 35 Å.

Upon increasing the Mg^{2+} concentration from 1 to 25 mM, the main population of the nc PEX-1ΔL4 precursor increases in mean P2–P4 distance from 62 to 64 Å, with $Mg_{1/2}$ of 0.35 mM (n=1.1), while the PEX-1ΔL4+J1/2 precursor decreases in mean P2-P4 distance from 52 to 49 Å, with $Mg_{1/2}$ of 2.2 mM (n=1.2; Figure 6A,C). Thus, the Mg^{2+} requirement for global folding is higher for PEX-1ΔL4+J1/2 than for PEX-1ΔL4 and the impact of Mg^{2+} on the two structures is distinct. The 3′P forms of both PEX-1ΔL4 and PEX-1ΔL4+J1/2 do not significantly change in mean P2–P4 distance over the entire Mg^{2+} range, remaining at approximately 68 and 66 Å, respectively. Therefore, the lack of J1/2 in construct PEX-1ΔL4+J1/2 amplifies the difference between precursor and 3′P in mean P2–P4 end-to-end distance relative to that of construct PEX-1ΔL4. Additional information obtained from time-resolved FRET is the full width at half-maximum (FWHM) of the distance distribution. Since the doubly labeled 3′-segment is shared between the two constructs, we can attribute qualitative differences in FWHM primarily to the intrinsic global flexibility of the RNA (Rueda et al., 2003; Tinsley et al., 2004). Figure 6B,D indicates that, upon addition of Mg^{2+}, changes in structural flexibility between the two constructs are different, where increasing Mg^{2+} concentrations decrease the structural flexibility of the PEX-1ΔL4 precursor and 3′P, as well as the PEX-1ΔL4+J1/2 3′P, but increase the flexibility of the PEX-1ΔL4+J1/2 precursor. Figure 7 summarizes our FRET results on the precursor and 3′P forms of the PEX-1ΔL4 and PEX-1ΔL4+J1/2 constructs under standard HDV ribozyme assay conditions (pH 7.5, 11 mM Mg^{2+}, 37°C).

Discussion

Up until approximately 25 years ago, all known enzymes were proteins. It was only then discovered that RNA is capable of enzymatic action in the form of ribozymes (Guerrier-Takada et al., 1983; Zaug et al., 1983). One advantage of ribozymes over their protein counterparts is that they can be separated into distinct strands and deterministically reassembled by Watson-Crick base pairing, providing for a convenient approach to the rational design of *trans*-acting ribozymes that specifically process chosen RNA targets in gene therapeutic applications (Sullenger and Gilboa, 2002; Breaker, 2004). The recent discovery of a large number of biologically relevant potential RNA targets, which appear to outnumber potential protein targets by several-fold (Carninci et al., 2005; Katayama et al., 2005), makes such an approach ever more attractive.

Recent advances have shown that changes in overall connectivity and topology, as required for designing a *trans*-acting ribozyme based on a naturally occurring autocatalytic or *cis*-acting form, often have a dramatic impact on the catalyzed rate constant (De la Pena et al., 2003; Khvorova et al., 2003; Zamel et al., 2004). The HDV ribozyme is no exception, as it shows ca. 10- to 100-fold lower cleavage activity in all *trans*-acting ribozymes when compared to the naturally occurring genomic and antigenomic forms (Pereira et al., 2002; Shih and Been, 2002; Tinsley et al., 2004). Previously, we showed that conformational rearrangements upon cleavage display the same trend of global extension along the P2–P4 helical axis in both *cis*- and *trans*-acting ribozymes; however, the conformational switch is significantly amplified in the *trans*-acting form (Tinsley et al., 2004). Here, we have generated a systematic set of four *cis*- and *trans*-acting HDV ribozymes to detect subtle structural and functional differences between constructs that differ only in the presence or absence of specific peripheral joining elements. We find that the removal of either capping loop L4 or helical crossover J1/2 significantly impacts catalytic activity (Figure 1). The effects of modifying the two peripheral joining elements are largely independent, as the activity loss of the doubly modified construct is characterized by a nearly additive increase in transition-state free energy. The Mg^{2+} dependence of cleavage shows that the construct retaining joiner J1/2 but not loop L4 displays the tight catalytic metal ion binding of the *cis*-acting form ($Mg_{1/2}$=ca. 1 mM), while the constructs lacking J1/2 (and L4) show significantly lower Mg^{2+} affinities (Figure 3), in all cases with low cooperativity between metal ions (n between 1 and 1.7). Structurally, we find that removal of joiner J1/2 renders the A-minor motif adjacent to the catalytically involved C76 residue more susceptible to terbium(III)-mediated backbone scission (Figure 4), lowers the binding affinity of the ribozyme for terbium(III) (Figure 5, Table 1), and significantly amplifies the magnitude of the global conformational change accompanying catalysis (Figures 2, 6 and 7). While removal of L4 has a similarly significant effect on catalytic activity as J1/2 removal, it appears to have a less dramatic effect on the global and local structure of the HDV ribozyme. These observations are consistent with a model in which removal of L4 and J1/2 act via distinct mechanisms to lower the catalytic activity of the HDV ribozyme over a significant distance (>20 Å, Figure 1) from the catalytic core. The helical crossover J1/2 is particularly important for conferring structural properties similar to those of the *cis*-acting ribozyme, and its removal induces greater dynamics and expansion of the catalytic core in

a way that impacts local and global folding, as well as catalytic function.

How do L4 and J1/2 exert their long-range influence on folding and function of the HDV ribozyme? Our terbium(III)-mediated footprinting suggests that removal of J1/2 renders the catalytic core more sensitive to the presence of the 5′-sequence, which we have previously shown to form a U-turn motif in the genomic HDV ribozyme (Sefcikova et al., 2007b) that wedges between the P2–P3 and P1–P1.1–P4 helical stacks (Ke et al., 2004; Krasovska et al., 2005). Therefore, removal of the connector J1/2, which tightly interlaces one end of the two helical stacks (Figure 1), likely results in larger fluctuations in the distance between and relative register of the helical stacks. Such a model of amplified inter-stack dynamics is consistent with the observed opening of the catalytic core to terbium(III)-mediated scission, the reduced metal ion affinity, and amplification of the global conformational change upon cleavage (i.e., upon dissociation of the 5′-sequence) in the absence of J1/2. Conversely, lower dynamics and tighter folding around the catalytic core in the presence of J1/2 is predicted to translate into faster cleavage rates and lower Mg^{2+} requirements, especially in the *cis*-acting ribozymes, presumably by reducing the entropic energy barrier of catalysis.

Perhaps the most surprising observation of the work described here is that removal of capping loop L4 also has a profound impact on catalytic efficiency of the HDV ribozyme, via a different mechanism than removal of J1/2. As a capping loop of a helix that projects away from the catalytic core, it is at least 30 Å removed from catalytic action and must exert any impact through the stable P4 stem with seven Watson-Crick base pairs (Figure 1). Our findings are consistent with earlier work on *trans*-acting ribozymes lacking L4, which revealed similar cleavage rate constants in the few min^{-1} range, approximately 10-fold lower than the rate of the *cis*-acting parent RNA (Luptak et al., 2001). Such long-range impact of a local change in topology is reminiscent of the dynamic structural rearrangements throughout the catalytic core of the hairpin ribozyme in response to site-specific chemical modification (Rhodes et al., 2006). It is thought that such structural communication is mediated by hydrogen bonding networks and van der Waals' packing, which connect distal parts of an RNA or protein by coupled motions to act as an interconnected whole (Benkovic and Hammes-Schiffer, 2003; Rueda et al., 2004; Hammes-Schiffer and Benkovic, 2006; Rhodes et al., 2006). In the case of removal of capping loop L4, the dynamics of helix P4 may be altered in a way that impacts the conformational equilibrium of the entire P1–P1.1–P4 stack, the integrity of which is known to be important for catalysis (Wadkins et al., 1999). Since the cleavage site G:U wobble pair is sandwiched between P1 and P1.1, such altered conformational dynamics may impact the catalytic core geometry in a way that decreases the rate (probability) of transition-state barrier crossing and thus catalysis. In this model the effect of L4 would mostly be exerted through the P1–P1.1–P4 stack, making it distinct from the impact of J1/2, which most likely acts through the relative orientation or register of the P1–P1.1–P4 and P2–P3 stacks. Such differential modes of catalytic interference caused by removal of loop L4 and joiner J1/2 would be most consistent with our experimental data. Our model deserves further testing, as it suggests an unexpectedly significant long-range impact of peripheral elements on the structure and function of biologically relevant RNAs such as the HDV ribozyme. It also holds the key to our ability to design more effective ribozymes for gene therapeutic applications.

Materials and methods

Preparation of RNA oligonucleotides

RNA oligonucleotides for constructs PEX-1ΔL4, PEX-1ΔL4+J1/2, and the substrate and 3′P strands for PEX-1ΔJ1/2 (Figure 1) were purchased from the Howard Hughes Medical Institute Biopolymer/Keck Foundation Biotechnology Resource RNA Laboratory at the Yale University School of Medicine (New Haven, CT, USA) and were purified as previously described (Pereira et al., 2002; Walter, 2002). The unmodified 3′P form of construct PEX-1, the substrate strand of PEX-1ΔL4, and the ribozyme strand of PEX-1ΔJ1/2 were generated by run-off transcription from a double-stranded, PCR-amplified template that encoded an upstream T7 promoter. Transcription reactions contained 40 mM Tris-HCl (pH 7.5), 15 mM $MgCl_2$, 5 mM dithiothreitol (DTT), 2 mM spermidine, 4 mM each rNTP, 5 U/ml inorganic pyrophosphatase, and 0.1 mg/ml T7 RNA polymerase and were incubated at 37°C overnight (ca. 16 h). The RNA was isolated after denaturing (8 M urea) 10% (w/v) polyacrylamide gel electrophoresis by UV shadowing, diffusion elution of small gel slices, and ethanol precipitation.

For cleavage reactions, the radiolabeled precursor form of PEX-1 was transcribed as described above, except that 0.04 mCi of [α-^{32}P]GTP and 0.125 μg/μl DNA oligonucleotide was added to the reaction mixture. This DNA oligonucleotide has a sequence fully complementary to the 15 nucleotides at the 5′-end of the precursor (G_{-7} to C_8) and was used to increase the yield of the uncleaved precursor RNA (Wadkins and Been, 1997). For the other constructs, 5′-^{32}P-labeled substrates were prepared by phosphorylation with T4 polynucleotide kinase and [γ-^{32}P]-ATP. Unless otherwise noted, unlabeled strands were added at a saturating 800 nM excess (3′-segment PEX-1B of construct PEX-1ΔL4+J1/2 at 1600 nM) in all assays.

Terbium stock solutions

The highest-purity terbium(III) chloride (99.9%) was purchased from Sigma-Aldrich (St. Louis, MO, USA). $TbCl_3$ stock solutions were prepared at 100 mM in 5 mM cacodylate (pH 5.5) and stored in small aliquots at -20°C to prevent formation of insoluble hydroxide species.

Gel mobility shift assays

Gel mobility shift assays were similar to those previously described (Pereira et al., 2002; Jeong et al., 2003). Briefly, nondenaturing 10% (w/v) polyacrylamide (19:1 acrylamide/bisacrylamide ratio) gels containing 50 mM Tris-HOAc (pH 7.5), 25 mM MES, 25 mM acetic acid and 11 mM $Mg(OAc)_2$ were assembled in the electrophoresis unit and equilibrated to 4°C for at least 2 h. 3′-^{32}P-labeled nc or self-cleaved PEX-1 or ribozyme or substrate strand was prepared by ligation with [^{32}P]pCp using T4 RNA ligase, followed by desalting through a CentriSep spin column (Princeton Separations, Adelphia, NJ, USA). The radiolabeled RNA (50 000 cpm) was pre-annealed in buffer of 5 mM Tris-OAc (pH 7.5) and 0.5 mM spermidine, either alone or with corresponding strands, denatured for 3 min at 90°C, and preincubated at 37°C for 10 min. The reactions were adjusted to

their final pH with a buffer containing 25 mM acetic acid, 25 mM MES, and 50 mM Tris-OAc (pH 7.5). These mixtures were incubated for an additional 5 min, after which 0.1 volumes of 110 mM $Mg(OAc)_2$ was added to a final concentration of 11 mM. The ribozyme was incubated for an additional 5 min. These samples were loaded on the gel, and an electric field of 8 V/cm was immediately applied. After typically 15–24 h of electrophoresis, the gel was exposed overnight and quantified using a PhosphorImager Storm 840 with ImageQuant software (Molecular Dynamics, Sunnyvale, CA, USA).

For FRET gel mobility assays of PEX-1ΔL4 and PEX-1ΔL4+J1/2, doubly fluorophore-labeled ribozyme strand B (10 pmol) was annealed to strand A (50 pmol for PEX-1ΔL4+J1/2) and/or the substrate strand (50 pmol for PEX-1ΔL4 and 100 pmol for PEX-1ΔL4+J1/2) and prepared as described above. The gel was scanned between low-fluorescence glass plates in a FluorImager SI fluorescence scanner with ImageQuant software (Molecular Dynamics) as previously described (Pereira et al., 2002; Jeong et al., 2003).

Cleavage activity assays

Radiolabeled precursor or ribozyme strands with 5′-[^{32}P]-labeled substrate strands were heated to 90°C for 2 min in a buffer containing 5 mM Tris-HCl (pH 7.5), 0.5 mM spermidine. The reactions mixtures for PEX-1ΔL4, PEX-1ΔJ1/2, and PEX-1ΔL4+J1/2 were supplemented with 0.1 mM EDTA. The precursor was then preincubated at 37°C for 10 min, after which the reactions were adjusted to the final pH (7.5) with a buffer containing 25 mM acetic acid, 25 mM MES, 50 mM Tris-HCl. These mixtures were incubated for an additional 5 min at 37°C, followed by addition of 0.25 volumes of a solution (also at 37°C) containing 55 mM $MgCl_2$ and 0.5 mM spermidine to start the reaction (Wadkins et al., 2001). Cleavage kinetics were followed by removing aliquots (2.5 or 5 μl) at specified times and quenching with 10 μl of 80% (v/v) formamide, 0.025% (w/v) xylene cyanol, and 0.025% (w/v) bromophenol blue, and 100 mM EDTA. In some cases, the quenching buffer was supplemented with 7 M urea to completely suppress cleavage. The reaction products were separated from the precursor by gel electrophoresis under denaturing conditions [8 M urea, 10% or 20% (w/v) polyacrylamide gels], quantified, and normalized to the sum of the precursor and 3′P bands using PhosphorImager Storm 840 with ImageQuant software (Molecular Dynamics). Time traces of product formation were fit with the single-exponential first-order rate equation $y=y_0+A(1-e^{-\tau/t})$, employing Marquardt-Levenberg non-linear regression (Igor Pro 5.03, Wavemetrics, Oswego, OR, USA), where A is the amplitude and τ^{-1} is the (pseudo-)first-order rate constant k_{obs}. To obtain bimolecular cleavage rate constants, the ribozyme concentration was varied from 12.5 to 800 nM for PEX-1ΔL4, from 50 to 1600 nM for PEX-1ΔJ1/2, and from 50 to 2000 nM for PEX-1ΔL4+J1/2; the rate constants k_{obs} of the ribozyme dependence were fit to the following binding equation:

$$k_{obs}=k_{cleav}\frac{[Rz]}{[Rz]+Rz_{1/2}}. \quad (1)$$

Similarly, the rates for Mg^{2+} dependence were fit to the following cooperative binding equation:

$$k_{obs}=A_0+k_{max}\frac{[Mg^{2+}]^n}{[Mg^{2+}]^n+Mg^n_{1/2}}, \quad (2)$$

yielding the cleavage rate constant k_{cleav} under standard conditions, the ribozyme and metal ion half-titration points $Rz_{1/2}$ and $Mg_{1/2}$, respectively, and the cooperativity coefficient n.

Terbium(III)-mediated footprinting

To observe the slow backbone scission mediated by $Tb(OH)(aq)^{2+}$, purified 3′-segments of PEX-1ΔL4, PEX-1ΔJ1/2, and PEX-1ΔL4+J1/2 were 5′ ^{32}P-phosphorylated with T4 polynucleotide kinase and [α-^{32}P]ATP, repurified by denaturing (8 M urea) 10% (w/v) polyacrylamide gel electrophoresis, followed by diffusion elution into 1 mM EDTA, and by ethanol precipitation. The labeled RNA strand (250 000 cpm per 10-μl reaction volume) was preannealed with the remaining unlabeled strand(s) in buffer (5 mM Tris-HCl, pH 7.5, 0.5 mM spermidine) by denaturation at 90°C for 3 min, followed by incubation at 37°C for 10 min. To form the RNA tertiary structure, Mg^{2+} was added 5 min prior to the addition of either 1 or 5 mM Tb^{3+} (final concentration) and the reaction was incubated for 1 h at 37°C. The scission reaction was stopped by addition of 50 mM EDTA (pH 8.0) and ethanol precipitation at -20°C. The precipitated RNA was redissolved in urea loading buffer [80% (v/v) formamide, 0.025% (w/v) xylene cyanol, 0.025% (w/v) bromophenol blue, 50 mM EDTA] and analyzed on a denaturing (7 M urea) wedged 20% (w/v) polyacrylamide sequencing gel alongside sequencing ladders from partial digestion with G-specific RNase T1 and alkaline hydrolysis as previously described (Walter et al., 2000; Harris and Walter, 2003, 2005). Product bands were visualized using a PhosphorImager Storm 840 with ImageQuant software (Molecular Dynamics) and a line fit was performed. The intensity was normalized and plotted as a function of the lane position in pixels.

Terbium(III) luminescence measurements

Steady-state luminescence spectra of terbium(III) bound to the pre-annealed and equilibrated 3′P forms of all of the constructs (1 μM) in standard reaction buffer (25 mM acetic acid, 25 mM MES, 50 mM Tris-HCl, pH 7.5, 11 mM $MgCl_2$) at 37°C were measured on an Amino-Bowman Series 2 (AB2) spectrofluorimeter (Thermo Spectronic, Madison, WI, USA), while slowly increasing the Tb^{3+} concentration over several orders of magnitude using appropriate stock solutions. After each terbium(III) addition, the solution was equilibrated for 5–10 min until the signal had stabilized before an emission spectrum was recorded. Excitation was at 290 nm (slit width 8 nm), and steady-state emission was scanned with a slit width of 8 nm. To extract the luminescence intensity of the major peak at 545 nm, each peak was fit between 535 and 555 nm using the following Gaussian distribution function:

$$y=y_0+\frac{A}{W\sqrt{\pi/2}}e^{-2\frac{(x-x_0)^2}{w^2}} \quad (3)$$

to yield the peak height as the pre-exponential factor, from which the background value in the absence of Tb^{3+} was subtracted. These signals were plotted over varying terbium(III) concentrations ($[Tb^{3+}]$) and fit to the Hill equation:

$$y=y_{max}\frac{[Tb^{3+}]^n}{[Tb^{3+}]^n+Tb^n_{1/2}} \quad (4)$$

to yield an apparent terbium(III) dissociation constant $Tb_{1/2}$ and a cooperativity or Hill constant n. For a fit over the entire terbium(III) titration range, a sum of two independent Hill equations produced the best result, as judged by the χ^2 deviation and residuals.

Time-resolved FRET measurements

The global structures of the PEX-1ΔL4 and PEX-1ΔL4+J1/2 HDV ribozymes were studied under standard conditions and as

a function of Mg^{2+} concentration by time-resolved FRET analysis of ribozyme complexes doubly labeled with fluorescein and tetramethylrhodamine, essentially as previously described (Pereira et al., 2002; Rueda et al., 2003). Briefly, the ribozyme-substrate (analog) or -3′P complex (75 μl; 1 μM doubly labeled ribozyme strand B, 5 μM strand A, and either 10 μM substrate, nc substrate analog, or 3′P), annealed by heating to 70°C for 2 min and cooled to room temperature, was incubated at 25°C for at least 15 min in standard buffer supplemented with 25 mM DTT and Mg^{2+}, as indicated. A frequency-doubled Nd:YVO_4 Millenia Xs-P laser (Spectra-Physics, Mountain View, CA, USA), operated between 8 and 8.5 W, pumped a frequency-doubled, mode-locked Ti:sapphire laser (Spectra-Physics, operated at 1 W) that excited fluorescein at 492 nm with pulses of 2 ps in width, picked down to 4 MHz. Detection of isotropic emission to >40 000 peak counts was performed under magic angle polarizer conditions at 520 nm (10-nm band-pass interference filter). Using a microchannel plate photomultiplier tube (Hamamatsu R3809U-50, Hamamatsu, Bridgewater, NJ, USA) feeding into an SPC-630 time-correlated single-photon counting card (Becker & Hickl, Berlin, Germany), decays were collected into 4096 channels with a time increment of 12.20 ps/channel. The instrument response function was measured as the scattering signal from a dilute solution of non-dairy coffee creamer to deconvolute the fluorescence decay data. To measure donor-acceptor distances, two time-resolved fluorescence decays were collected, with and without acceptor in place. The fluorescein emission decay in the donor-only complex was used to extract the two or three intrinsic donor lifetimes τ_i with their fractional contributions α_i by a sum-of-exponentials fit. Data from the doubly labeled complex $I_{DA}(t)$ were then fit to the equation:

$$I_{DA}(t) = \sum_k f_k \int P_k(R) \sum_i \alpha_i \exp\left\{-\frac{t}{\tau_i}\left[1+\left(\frac{R_0}{R}\right)^6\right]\right\} dR, \quad (5)$$

where the first sum refers to the number of distributions, either one or two, each with fractional population f_k and distance distribution $P_k(R)$. Distance distributions were modeled as weighted three-dimensional Gaussian functions and fit to the equation:

$$P(R) = 4\pi R^2 c \exp[-a(R-b)^2], \quad (6)$$

where a and b are parameters that describe the shape of the distribution and c is a normalization constant. Fitting was performed by nonlinear least-squares regression, with a, b, and f_k for each distribution as adjustable parameters. An additional adjustable parameter was a small fraction of singly labeled complex (always <5%), accounting for photobleached acceptor fluorophore.

Mg^{2+} was titrated by incremental addition of 0.5-μl aliquots of appropriate $MgCl_2$ stock solutions in standard buffer supplemented with 25 mM DTT, taking into account the volume change; the volume at the end of any given titration increased by not more than 10%. In all cases, distance distribution fits were judged as good when a low (<1.2) reduced χ^2 value and evenly distributed residuals were obtained. To extract absolute distances, a value of 55 Å for the Förster distance R_0 of fluorescein and tetramethylrhodamine was used, assuming a value of $^2/_3$ for the orientation factor based on the high mobility of the fluorophores, as evident from their low fluorescence anisotropy. The Mg^{2+} concentration dependence of the helix P2–P4 distance was fit with Eq. (2).

Acknowledgments

The authors wish to thank Hashim Al-Hashimi, Carol Fierke, and the members of the Walter laboratory for stimulating discussions. This work was supported by NIH Grant GM62357 (N.G.W.) and an NIH NRSA Pre-doctoral fellowship (R.A.T.).

References

Been, M.D. (2006). HDV ribozymes. Curr. Top. Microbiol. Immunol. *307*, 47–65.

Benkovic, S.J. and Hammes-Schiffer, S. (2003). A perspective on enzyme catalysis. Science *301*, 1196–1202.

Breaker, R.R. (2004). Natural and engineered nucleic acids as tools to explore biology. Nature *432*, 838–845.

Carninci, P., Kasukawa, T., Katayama, S., Gough, J., Frith, M.C., Maeda, N., Oyama, R., Ravasi, T., Lenhard, B., Wells, C., et al. (2005). The transcriptional landscape of the mammalian genome. Science *309*, 1559–1563.

D'Anjou, F., Bergeron, L.J., Larbi, N.B., Fournier, I., Salzet, M., Perreault, J.P., and Day, R. (2004). Silencing of SPC2 expression using an engineered delta ribozyme in the mouse βTC-3 endocrine cell line. J. Biol. Chem. *279*, 14232–14239.

Das, S. and Piccirilli, J. (2005). General acid catalysis by the hepatitis delta virus ribozyme. Nat. Chem. Biol. *1*, 45–52.

De la Pena, M., Gago, S., and Flores, R. (2003). Peripheral regions of natural hammerhead ribozymes greatly increase their self-cleavage activity. EMBO J. *22*, 5561–5570.

Doudna, J.A. and Lorsch, J.R. (2005). Ribozyme catalysis: not different, just worse. Nat. Struct. Mol. Biol. *12*, 395–402.

Fedor, M.J. and Williamson, J.R. (2005). The catalytic diversity of RNAs. Nat. Rev. Mol. Cell Biol. *6*, 399–412.

Fiola, K., Perreault, J.P., and Cousineau, B. (2006). Gene targeting in the Gram-positive bacterium *Lactococcus lactis*, using various delta ribozymes. Appl. Environ. Microbiol. *72*, 869–879.

Gondert, M.E., Tinsley, R.A., Rueda, D., and Walter, N.G. (2006). The catalytic core structure of the *trans*-acting HDV ribozyme is subtly influenced by sequence variation outside the core. Biochemistry *45*, 7563–7573.

Guerrier-Takada, C., Gardiner, K., Marsh, T., Pace, N., and Altman, S. (1983). The RNA moiety of ribonuclease P is the catalytic subunit of the enzyme. Cell *35*, 849–857.

Hammes-Schiffer, S. and Benkovic, S.J. (2006). Relating protein motion to catalysis. Annu. Rev. Biochem. *75*, 519–541.

Hargittai, M.R., Mangla, A.T., Gorelick, R.J., and Musier-Forsyth, K. (2001). HIV-1 nucleocapsid protein zinc finger structures induce tRNA(Lys,3) structural changes but are not critical for primer/template annealing. J. Mol. Biol. *312*, 985–997.

Hargittai, M.R. and Musier-Forsyth, K. (2000). Use of terbium as a probe of tRNA tertiary structure and folding. RNA *6*, 1672–1680.

Harris, D.A. and Walter, N.G. (2003). Probing RNA structure and metal-binding sites using terbium footprinting. Curr. Prot. Nucleic Acid Chem. *6.8*, 6.8.1–6.8.8.

Harris, D.A. and Walter, N.G. (2005). Terbium(III) footprinting as a probe of RNA structure and metal-binding sites. In: Handbook of RNA Biochemistry, R.K. Hartmann, A. Bindereif, A. Schön, and E. Westhof, eds. (Weinheim, Germany: Wiley-VCH), pp. 205–213.

Harris, D.A., Rueda, D., and Walter, N.G. (2002). Local conformational changes in the catalytic core of the trans-acting hepatitis delta virus ribozyme accompany catalysis. Biochemistry *41*, 12051–12061.

Harris, D.A., Tinsley, R.A., and Walter, N.G. (2004). Terbium-mediated footprinting probes a catalytic conformational switch in the antigenomic hepatitis delta virus ribozyme. J. Mol. Biol. *341*, 389–403.

Jeong, S., Sefcikova, J., Tinsley, R.A., Rueda, D., and Walter, N.G. (2003). *Trans*-acting hepatitis delta virus ribozyme: catalytic core and global structure are dependent on the 5′ substrate sequence. Biochemistry *42*, 7727–7740.

Katayama, S., Tomaru, Y., Kasukawa, T., Waki, K., Nakanishi, M., Nakamura, M., Nishida, H., Yap, C.C., Suzuki, M., Kawai, J., et al. (2005). Antisense transcription in the mammalian transcriptome. Science *309*, 1564–1566.

Ke, A., Zhou, K., Ding, F., Cate, J.H., and Doudna, J.A. (2004). A conformational switch controls hepatitis delta virus ribozyme catalysis. Nature *429*, 201–205.

Khvorova, A., Lescoute, A., Westhof, E., and Jayasena, S.D. (2003). Sequence elements outside the hammerhead ribozyme catalytic core enable intracellular activity. Nat. Struct. Biol. *10*, 708–712.

Krasovska, M.V., Sefcikova, J., Spackova, N., Sponer, J., and Walter, N.G. (2005). Structural dynamics of precursor and product of the RNA enzyme from the hepatitis delta virus as revealed by molecular dynamics simulations. J. Mol. Biol. *351*, 731–748.

Lai, M.M. (1995). The molecular biology of hepatitis delta virus. Annu. Rev. Biochem. *64*, 259–286.

Lilley, D.M. (2004). The Varkud satellite ribozyme. RNA *10*, 151–158.

Lucier, J.F., Bergeron, L.J., Briere, F.P., Ouellette, R., Elela, S.A., and Perreault, J.P. (2006). RiboSubstrates: a web application addressing the cleavage specificities of ribozymes in designated genomes. BMC Bioinformatics *7*, 480.

Luptak, A., Ferre-D'Amare, A.R., Zhou, K., Zilm, K.W., and Doudna, J.A. (2001). Direct pK_a measurement of the active-site cytosine in a genomic hepatitis delta virus ribozyme. J. Am. Chem. Soc. *123*, 8447–8452.

Macnaughton, T.B. and Lai, M.M. (2006). HDV RNA replication: ancient relic or primer? Curr. Top. Microbiol. Immunol. *307*, 25–45.

Nakano, S., Chadalavada, D.M., and Bevilacqua, P.C. (2000). General acid-base catalysis in the mechanism of a hepatitis delta virus ribozyme. Science *287*, 1493–1497.

Pereira, M.J., Harris, D.A., Rueda, D., and Walter, N.G. (2002). Reaction pathway of the *trans*-acting hepatitis delta virus ribozyme: a conformational change accompanies catalysis. Biochemistry *41*, 730–740.

Perrotta, A.T. and Been, M.D. (1998). A toggle duplex in hepatitis delta virus self-cleaving RNA that stabilizes an inactive and a salt-dependent pro-active ribozyme conformation. J. Mol. Biol. *279*, 361–373.

Perrotta, A.T., Shih, I., and Been, M.D. (1999). Imidazole rescue of a cytosine mutation in a self-cleaving ribozyme. Science *286*, 123–126.

Perrotta, A.T., Wadkins, T.S., and Been, M.D. (2006). Chemical rescue, multiple ionizable groups, and general acid-base catalysis in the HDV genomic ribozyme. RNA *12*, 1282–1291.

Rhodes, M.M., Reblova, K., Sponer, J., and Walter, N.G. (2006). Trapped water molecules are essential to structural dynamics and function of a ribozyme. Proc. Natl. Acad. Sci. USA *103*, 13380–13385.

Roy, G., Ananvoranich, S., and Perreault, J.P. (1999). Delta ribozyme has the ability to cleave *in trans* an mRNA. Nucleic Acids Res. *27*, 942–948.

Rueda, D., Bokinsky, G., Rhodes, M.M., Rust, M.J., Zhuang, X., and Walter, N.G. (2004). Single-molecule enzymology of RNA: essential functional groups impact catalysis from a distance. Proc. Natl. Acad. Sci. USA *101*, 10066–10071.

Rueda, D., Wick, K., McDowell, S.E., and Walter, N.G. (2003). Diffusely bound Mg2+ ions slightly reorient stems I and II of the hammerhead ribozyme to increase the probability of formation of the catalytic core. Biochemistry *42*, 9924–9936.

Salehi-Ashtiani, K., Luptak, A., Litovchick, A., and Szostak, J.W. (2006). A genomewide search for ribozymes reveals an HDV-like sequence in the human *CPEB3* gene. Science *313*, 1788–1792.

Sefcikova, J., Krasovska, M.V., Spackova, N., Sponer, J., and Walter, N.G. (2007a). Impact of an extruded nucleotide on cleavage activity and average catalytic core conformation of the HDV ribozyme. Biopolymers *85*, 392–406.

Sefcikova, J., Krasovska, M.V., Sponer, J., and Walter, N.G. (2007b). The genomic HDV ribozyme utilizes a previously unnoticed U-turn motif to accomplish fast site-specific catalysis. Nucleic Acids Res. *35*, 1933–1946.

Shih, I.H. and Been, M.D. (2001). Involvement of a cytosine side chain in proton transfer in the rate-determining step of ribozyme self-cleavage. Proc. Natl. Acad. Sci. USA *98*, 1489–1494.

Shih, I.H. and Been, M.D. (2002). Catalytic strategies of the hepatitis delta virus ribozymes. Annu. Rev. Biochem. *71*, 887–917.

Sullenger, B.A. and Gilboa, E. (2002). Emerging clinical applications of RNA. Nature *418*, 252–258.

Tinsley, R.A., Harris, D.A., and Walter, N.G. (2003). Significant kinetic solvent isotope effects in folding of the catalytic RNA from the hepatitis delta virus. J. Am. Chem. Soc. *125*, 13972–13973.

Tinsley, R.A., Harris, D.A., and Walter, N.G. (2004). Magnesium dependence of the amplified conformational switch in the *trans*-acting hepatitis delta virus ribozyme. Biochemistry *43*, 8935–8945.

Wadkins, T.S. and Been, M.D. (1997). Core-associated nonduplex sequences distinguishing the genomic and antigenomic self-cleaving RNAs of hepatitis delta virus. Nucleic Acids Res. *25*, 4085–4092.

Wadkins, T.S., Perrotta, A.T., Ferre-D'Amare, A.R., Doudna, J.A., and Been, M.D. (1999). A nested double pseudoknot is required for self-cleavage activity of both the genomic and antigenomic hepatitis delta virus ribozymes. RNA *5*, 720–727.

Wadkins, T.S., Shih, I., Perrotta, A.T., and Been, M.D. (2001). A pH-sensitive RNA tertiary interaction affects self-cleavage activity of the HDV ribozymes in the absence of added divalent metal ion. J. Mol. Biol. *305*, 1045–1055.

Walter, N.G. (2001). Structural dynamics of catalytic RNA highlighted by fluorescence resonance energy transfer. Methods *25*, 19–30.

Walter, N.G. (2002). Probing RNA structural dynamics and function by fluorescence resonance energy transfer (FRET). Curr. Prot. Nucleic Acid Chem. *11.10*, 11.10.11–11.10.23.

Walter, N.G., Burke, J.M., and Millar, D.P. (1999). Stability of hairpin ribozyme tertiary structure is governed by the interdomain junction. Nat. Struct. Biol. *6*, 544–549.

Walter, N.G., Yang, N., and Burke, J.M. (2000). Probing nonselective cation binding in the hairpin ribozyme with Tb(III). J. Mol. Biol. *298*, 539–555.

Winkler, W.C., Nahvi, A., Roth, A., Collins, J.A., and Breaker, R.R. (2004). Control of gene expression by a natural metabolite-responsive ribozyme. Nature *428*, 281–286.

Zamel, R., Poon, A., Jaikaran, D., Andersen, A., Olive, J., De Abreu, D., and Collins, R.A. (2004). Exceptionally fast self-cleavage by a *Neurospora* Varkud satellite ribozyme. Proc. Natl. Acad. Sci. USA *101*, 1467–1472.

Zaug, A.J., Grabowski, P.J., and Cech, T.R. (1983). Autocatalytic cyclization of an excised intervening sequence RNA is a cleavage-ligation reaction. Nature *301*, 578–583.

Received February 18, 2007; accepted April 13, 2007